

Reentrance effect in normal-metal/superconducting hybrid loops

C.-J. Chien and V. Chandrasekhar

Department of Physics and Astronomy, Northwestern University, Evanston, Illinois 60208

(May 26, 2022)

Abstract

We have measured the transport properties of two mesoscopic hybrid loops composed of a normal-metal arm and a superconducting arm. The samples differed in the transmittance of the normal/superconducting interfaces. While the low transmittance sample showed monotonic behavior in the low temperature resistance, magnetoresistance and differential resistance, the high transmittance sample showed reentrant behavior in all three measurements. This reentrant behavior is due to coherent Andreev reflection at the normal/superconducting interfaces. We compare the reentrance effect for the three different measurements and discuss the results based on the theory of quasiclassical Green's functions.

74.50.+r, 74.80.Fp, 73.23.-b

I. INTRODUCTION

The resistance of a normal metal (N) in contact with a superconductor (S) is modified in the vicinity of the N-S interface, a phenomenon well known as the superconducting proximity effect [1]. The microscopic mechanism of the proximity effect is Andreev reflection at the N-S interface: An electron in the normal metal with energy less than the gap of the superconductor is Andreev-reflected as a hole, with the concurrent generation of a Cooper pair in the superconductor [2]. The consequence of this mechanism is the existence of a superconducting correlation in the normal metal. Recently, using a theory based on quasiclassical nonequilibrium Green's functions, it was shown that the superconducting correlation is expected to decay over a length $\xi(\epsilon)=\sqrt{\hbar D_N/\epsilon}$, where ϵ is the energy of the electron and D_N the diffusion constant of electrons in the normal metal [3–8]. The surprising result was predicted that the resistance of the normal metal returns to its normal state value at zero temperature and energy, the so-called reentrance effect [3–8].

The physical manifestation of this reentrant behavior can be seen in the transport properties which are described by an effective diffusion constant $D(\epsilon, x)$, a quantity dependent on the energy of the electron ϵ and the position x [6–8]. $D(\epsilon, x)$ coincides with its normal state value at zero energy, increases and reaches a maximum at an intermediate energy of the order of the Thouless energy $E_c = \hbar D_N/L^2$, and coincides with its normal state value again at higher energies (L here is the length of the normal metal). As a function of temperature, the resistance of a diffusive normal metal adjacent to a superconductor shows a minimum at a temperature T of the order of E_c/k_B (where k_B is the Boltzmann constant), and regains its normal state value as $T \rightarrow 0$. A similar minimum is expected in the differential resistance of the normal metal as a function of dc voltage V . If the diffusive normal metal is connected to two superconductors with different phases, the resistance is expected to oscillate as a function of the phase difference between the superconductors, which can be modulated by the application of a magnetic field. The amplitude of the magnetoresistance oscillations shows a maximum when T is of the order of E_c/k_B and vanishes again as $T \rightarrow 0$.

(neglecting electron-electron interaction in the normal metal) [6–8]. All this is strictly valid only for high interface transmittances; if the interface transmittance is low, the probability of Andreev reflection is correspondingly reduced, and the reentrant behavior in the transport properties is shifted to lower energy scales, and may disappear entirely [5,9].

Several groups have reported observing this reentrance effect in normal metal-superconductor (N-S) or semiconductor-superconductor (Sm-S) structures. In N-S structures, Courtois *et al.* [10] reported observing magnetoresistance oscillations in a normal Cu loop with two superconducting Al islands on either side. No reentrant behavior was observed, however, possibly because it was masked by the Josephson coupling between the superconducting islands. Charlat *et al.* [11] observed the reentrance effect as a function of both temperature and voltage in a Cu loop adjacent to a small superconducting Al island. In a different geometry, Petrashov *et al.* [12] observed the reentrance effect in the amplitude of magnetoresistance oscillations in an Andreev interferometer. In Sm-S structures, den Hartog *et al.* [13,14] have reported observing reentrant behavior in a geometry where a diffusive two dimensional electron gas is coupled to a superconductor to form a loop. In these experiments, den Hartog *et al.* observed reentrant behavior not only in the resistance as a function of dc voltage, but also in the amplitude of magnetoresistance oscillations as a function of dc voltage. Toyoda *et al.* [15] observed reentrance in the magnetoresistance oscillations of a two dimensional electron gas connected to a superconducting loop. While the results of these experiments qualitatively agree with the theory, quantitative comparison with theory is still not satisfactory, especially at high energies or temperatures close to T_c , where quantitative predictions are difficult to obtain.

In this paper, we report detailed transport measurements on two N-S devices as a function of temperature T , magnetic field H and dc voltage bias V . Both devices are in the form of square loops, with one arm of the loop fabricated from a normal metal (Ag or Au) and the remaining three arms from a superconductor (Al). The primary difference between the two samples is in the transmittance of the N-S interfaces: One sample (sample A) has low interface transmittances ($R_b/R_N > 1$, where R_b is the interface resistance and R_N is

resistance of the normal metal), while the other sample (sample B) has high interface transmittances ($R_b/R_N \ll 1$). Both samples show a strong temperature dependent resistance $R(T)$, large oscillations in the magnetoresistance $R(H)$, and a differential resistance dV/dI which is a function of V below the critical temperature T_c of the superconductor. While sample A shows monotonic behavior in all three measurements, sample B shows reentrant behavior in $R(T)$, $dV/dI(V)$, and amplitude of oscillations in $R(H)$ as a function of T . The temperature and energy scales for this reentrant behavior are in qualitative agreement with recent theories on Andreev reflection in mesoscopic N-S devices [3–8], although detailed quantitative agreement is still lacking.

II. SAMPLE FABRICATION AND MEASUREMENT

An electron beam micrograph of sample A is shown in Fig. 1(a), and schematics of the two samples A and B are shown in Fig. 1(b). The samples were fabricated by a conventional multi-level electron-beam lithography process. The normal metal was deposited first. After a second level of e-beam lithography, the normal metal surface was cleaned by a dc Ar^+ etch and the superconductor (Al) was deposited without breaking vacuum in order to ensure good contacts between N and S. Au was used as the normal metal for sample A, while Ag was used for sample B. Control Ag and Al wires were coevaporated with sample B in order to calibrate film properties. The relevant film parameters are as follows: Au/Ag thickness ~ 28 nm, Al thickness ~ 37 nm, wire linewidth $\sim 0.1 - 0.14 \mu m$, normal metal (Ag) coherence length $\xi_N(T) \sim 0.23 \mu m / \sqrt{T}$, superconducting coherence length $\xi_{Al}(T = 0) = 0.31 \mu m$, and electron phase coherence length $L_\varphi = 0.9 \mu m$ at $T=30$ mK [19]. The area of the N-S interfaces was approximately $0.15 \times 0.15 \mu m^2$. The samples were measured in a dilution fridge between 30 mK and 1.5 K using a four-terminal ac resistance bridge, with ac excitations in the range of 10-100 nA, small enough to avoid self-heating. The four terminal measurement configuration is shown in Fig 1(b). For the dV/dI measurements, the dc current was applied through the same leads as the ac current. Aside from the transparency of the interfaces, the

major difference between the two samples is the greater length of the normal metal arms beyond the loop in sample A in comparison to sample B (see Fig. 1(b)).

III. EXPERIMENTAL RESULTS

Figure 2 shows the resistance of both samples as a function of temperature. The first difference noticeable between the two samples can be seen near T_c . For sample B, there is a sharp drop in resistance as the sample is cooled through T_c . If the N-S interface resistances were negligible, one might expect the superconducting arm to short out the normal arm of the loop, resulting in a decrease in resistance corresponding to the normal state resistance of the loop alone. This is indeed the change in resistance we observe for sample B within our experimental error, based on the measured resistivities of the normal metal and superconductor. Thus, the interface in sample B appears to be highly transparent. Since the resistance of sample A does not show a sharp drop at T_c , but only a gradual and small decrease as the temperature is lowered, we conclude that the interface transmittances for this sample are small. We can also estimate the barrier resistance from the resistivities of the Ag, Au and Al films along with the measured resistance of the samples. Based on these measurements, the resistance of each N-S interface is $\sim 25 \Omega$ for sample A and $< 0.5 \Omega$ for sample B.

The second major difference between the two samples is seen in the low temperature behavior. When the temperature is reduced from $T = 1.2 \text{ K}$ to 30 mK , the resistance of sample A decreases monotonically. Sample B, on the other hand, eventually shows an *increase* in the resistance, resulting in a minimum in the resistance at $\sim 520 \text{ mK}$. This is similar to the behavior observed by Charlat *et al.* [11] in their Cu/Al loops, and was attributed by them to the anomalous proximity effect in the Cu loop induced by the Al island. The temperature at which the resistance minimum R_{min} occurs is given approximately by the temperature at which $\xi_N(\epsilon = k_B T)$ is comparable to length of the relevant normal region. For sample B, the normal regions that contribute to the low temperature zero bias

resistance are the small normal arms outside the loop, which have lengths of 0.15 and 0.55 μm respectively, since the loop itself has zero resistance below T_c . The resistance at the lowest temperature is 5.9 Ω which corresponds to the resistance of the normal side branches at this temperature as noted above. Due to its longer length, the contribution from the 0.55 μm arm should dominate the electrical transport. The temperature corresponding to the Thouless energy for this arm is $T = E_c/k_B \sim 170$ mK, a factor of 3 lower than the measured temperature of ~ 520 mK. However, it should be noted that for a normal wire with one end connected to a superconducting reservoir and the other end to a normal reservoir, the minimum is expected to occur at $T \sim 5E_c/k_B$ [4,6]. For sample A, the absence of reentrant behavior is consistent with the fact the interface transmittances in this sample are small. In addition, the normal side arms are long, and would not be expected to show reentrant behavior in our temperature range. If one considers the normal region in the immediate vicinity of the low transmission interface as a highly disordered conductor with a very low diffusion coefficient D , the relevant $\xi_N(T)$ is very short, and hence the reentrant behavior is pushed to much lower energies and temperatures [5,13].

A similar difference between the two samples can be observed by examining the magnetoresistance oscillations as a function of temperature. Figure 3(a) shows the magnetoresistance of sample A at a few temperatures below 1 K. Oscillations of a period corresponding to a flux $h/2e$ through the loop are observed which persist up to the critical temperature T_c of the superconductor, and whose amplitude at the lowest temperatures is much larger than e^2/h (in terms of conductance). Similar oscillations are seen in sample B (Fig. 3(b)). The presence of magnetoresistance oscillations points to the existence of a quantum interference effect involving the doubly-connected loop. The large amplitude of these oscillations rules out the possibility of their being due to a normal metal quantum interference effect such as weak localization or conductance fluctuations, whose amplitude is typically $\sim e^2/h$, and points to a coherent interference phenomenon involving charge carriers in the normal and superconducting arms of the loop [20–23].

Figure 3(c) shows the amplitude of the magnetoresistance oscillations for the two samples

as a function of temperature. The amplitude is determined by calculating the power in the Fourier transform in the inverse field range corresponding to the area of the loop, over the field range ± 25 mT for sample A and ± 20 mT for sample B. While the oscillation amplitude in sample A shows a monotonic increase as the temperature is decreased, the amplitude of the oscillations for sample B displays reentrant behavior with a maximum at a temperature of ~ 200 mK. Since the oscillations arise from interference effects around the loop, one might expect that the amplitude of the oscillations would be determined by the ratio of $\xi_N(\epsilon = k_B T)$ to half the length L of the normal arm, which is $\sim 1.1 \mu m$. At $T \sim 170$ mK, $2\xi_N(\epsilon = k_B T) = L$. This is in good agreement with the temperature at which we observe the amplitude maximum. For sample A, no such maximum is observed, even though the film parameters for the two samples are similar. This again is a consequence of the low N-S interface transparencies in this sample. At higher temperatures, both samples show a temperature dependence which is well described by a function of the form $\exp[-\alpha L/\xi_N(T)]$, as can be seen in Fig. 3(c). This is in contrast to the results of Courtois *et al.* [10], where the magnetoresistance oscillations were seen to decay as a power law in temperature. For comparison, we also show the best fit to the power law dependence found in Ref. [10], which does not describe the data well. This difference may arise from the difference in the geometry of the samples in the two experiments.

The differential resistance dV/dI as a function of V of sample A and sample B also show differences which are consistent with the difference in the quality of their interfaces. Figure 4 shows dV/dI as a function of V for both samples at low temperature and bias. Sample B again shows reentrant behavior, with a resistance minimum at a bias voltage of $\sim 7.25 \mu V$. As in the temperature dependent resistance, only the two normal side arms are expected to contribute at low dc bias. E_c for the longer arm is $15 \mu eV$, and hence the voltage at the resistance minimum is *smaller* than expected by approximately factor of two. This should be contrasted with the temperature dependence of this sample which was discussed earlier, where the temperature at which the minimum in resistance was observed was *larger* than E_c/k_B by a factor of three. This discrepancy will be discussed later when we attempt to

compare these data with the quasiclassical Green's function theory.

In contrast to sample B, sample A shows only a gradual increase in resistance at zero field with voltage, consistent with the behavior seen in the temperature dependence. At a finite magnetic field of 225 gauss, the curvature of the peak changes, and dV/dI as a function of V shows what appears to be reentrant behavior as a function of voltage, similar to that of sample B. However, this change in the curvature is not due to reentrance, which can be seen by examining the temperature dependence of the sample in a finite magnetic field. Figure 5(a) shows the temperature dependent resistance of sample A at four different magnetic fields corresponding to 0, $1/2$, 1 and $3/2$ flux quanta $h/2e$ through the area of the loop. Although the curves for half-integral flux quanta are different from those for integral flux quanta, no reentrant behavior is observed. We believe instead that the change in curvature is similar to the zero bias anomaly behavior observed by Kastalsky *et al.* [25], which was explained by van Wees *et al.* [26] as arising from suppression of coherent multiple Andreev reflections by a magnetic field. Figure 5(b) shows similar data for sample B, where curves for both integral and half-integral flux quanta show clear reentrant behavior. At half-integral flux quanta, there is a small increase in the temperature T_{min} at which the resistance minimum occurs, but the curve for zero and one flux quantum are almost the same. This is in contrast to the results of Charlat *et al.* [11], who saw a monotonic increase in T_{min} as the magnetic field was increased which they attributed to the field dependence of the electron phase coherence length L_φ . At finite magnetic field, L_φ is shorter than at zero field [32]. Since L_φ defines the cutoff length for coherent Andreev reflection, L_φ corresponds to the effective length of the sample, and hence the minimum in resistance as a function of temperature would move to higher temperatures as a function of magnetic field. This is clearly not seen in our samples.

IV. DISCUSSION

A. Quasiclassical Green's function model

We shall now attempt a quantitative description of the temperature and voltage dependences of sample B using the quasiclassical Green's function theory. Our analysis is based on solving the Usadel equation [27] for the parametrized pair correlation function $\theta(\epsilon, x)$ in the normal metal [3–8]. $\theta(\epsilon, x)$ is a function of the energy ϵ and position x . Assuming that the electron phase coherence length L_φ is much longer than the length of the normal metal, the Usadel equation can be written in the simplified form

$$\frac{\partial^2 \theta(\epsilon, x)}{\partial x^2} + 2i\epsilon \sin \theta(\epsilon, x) = 0 \quad (1)$$

The current is then given by the equation developed in Ref. [8] (for the special case of a perfect interface):

$$I(V, T) = \frac{1}{2R_N} \int_0^\infty d\epsilon \left[\tanh \left(\frac{\epsilon + eV}{2k_B T} \right) - \tanh \left(\frac{\epsilon - eV}{2k_B T} \right) \right] D(\epsilon) \quad (2)$$

where $D(\epsilon)$ is the energy dependent diffusion coefficient in the normal metal which is given in terms of $\theta(\epsilon, x)$ by

$$D(\epsilon) = \frac{1}{\frac{1}{L} \int_0^L dx \operatorname{sech}^2 [Im \theta(\epsilon, x)]} \quad (3)$$

The conductance is obtained from Eq. (2) by taking the derivative with respect to the voltage V , $G(V, T) = dI/dV$. At zero bias, the calculation is simplified and the following formula is obtained for the resistance $R(T)$:

$$R(T) = R_N \left[\int_0^\infty \frac{d\epsilon}{2k_B T \cosh^2 \frac{\epsilon}{2k_B T}} \frac{1}{\frac{1}{L} \int_0^L dx \operatorname{sech}^2 [Im \theta(\epsilon, x)]} \right]^{-1} \quad (4)$$

Equation (1) must be solved subject to the appropriate boundary conditions, which are usually specified at the N and S reservoirs [5,6,8]. At a N reservoir, $\theta(\epsilon, x) = 0$. At a S reservoir,

$$\theta(\epsilon, x) = \frac{\pi}{2} + i \frac{1}{2} \ln \left[\frac{\Delta + \epsilon}{\Delta - \epsilon} \right] \quad (5a)$$

for $\epsilon < \Delta$, and

$$\theta(\epsilon, x) = i\frac{1}{2}\ln\left[\frac{\epsilon + \Delta}{\epsilon - \Delta}\right] \quad (5b)$$

for $\epsilon > \Delta$, where Δ is the superconducting energy gap. At the N-S interface,

$$\sigma_{N,S}S\left[\frac{\partial\theta(\epsilon, x)}{\partial x}\right] = G_b\sin[\theta_s(L, \epsilon) - \theta_N(L, \epsilon)] \quad (5c)$$

where $\sigma_{N,S}$ is the conductivity of the interface, S is the cross section of the wire and G_b is the conductance of the interface. Finally, at a node where two or more normal wires intersect, the boundary condition is determined by a Kirchoff-like equation of the form

$$\sum_i S_i \frac{\partial\theta(\epsilon, x)}{\partial x} = 0 \quad (5d)$$

where S_i denotes the cross section of the branch i joining the node [8].

Conceptually, at least, determining the resistance of any arbitrary sample is a straightforward matter: one solves the Usadel equation for the pair amplitude $\theta(\epsilon, x)$ subject to the appropriate boundary conditions, then substitutes the result into either Eq. (2) or (4). Practically, however, the Usadel equation needs to be solved numerically. This is not easy, particularly for complicated structures such as our Andreev interferometers, and we make certain simplifying assumptions to make the calculation tractable. Fig. 6(a) shows a schematic of sample B. As we have noted earlier, we assume that the N-S interface resistances are very small, so that the loop resistance is zero, as it is shorted by the superconducting arm. The measured normal-metal resistance R is then simply the sum of the two N side branches, R_1 and R_2 . To determine the resistance of these structures in the proximity effect regime, we need to solve the Usadel equation in the one dimensional wires on either side of the loop. Since the electron phase coherence length L_φ places an upper cutoff to the pair correlation in the normal metal, we take the normal reservoirs to be at a distance L_φ from the superconductor. Finally, our calculations show that the effect of the voltage probes on $\theta(\epsilon, x)$ in the side arms of the structure is very small, and hence we ignore the effect of these probes.

Figure 6(b) shows the final N-S-N geometry that we simulate based on the procedure developed in Refs. [5,6,8]. If we consider the superconductor to be at zero voltage, the

energy ϵ of the quasiparticles in each branch i of the structure is related to the voltage drop V_i between the corresponding normal reservoir and the superconductor by $\epsilon_i = eV_i$. However, due to the four terminal nature of our measurements, the voltage that is actually measured is the voltage $V_2 - V_1$ at the voltage probes. Although the potential profile in the one dimensional normal wire between the normal and superconducting reservoirs is not predicted to be linear [28], the deviations from linearity are small enough that we can relate the voltages measured at each probe to the voltage V at the corresponding normal reservoir by a linear scaling of the form $V_i = V(L_i/L_\varphi)$, where L_i is the length of the arm from the superconductor to the point at which the voltage probe joins the wire. (L_φ is the effective distance to the corresponding normal reservoir.) Furthermore, to calculate the resistance of each branch, we need to use Eq. (4), but with the integral over the length L restricted to L_i for each branch, and the normal state resistance R_N corresponding to the normal state resistance R_{Ni} for each arm. The total temperature dependent resistance of the sample is then the sum of the resistances $R_1(T)$ and $R_2(T)$.

B. Temperature dependence

Figure 7(a) shows $R_1(T)$, $R_2(T)$, and the sum $R_1(T) + R_2(T)$ calculated in the limit $\Delta \gg E_c$ for the temperature regime below 1 K. As expected, the major contribution to the resistance comes from the longer ($0.55 \mu m$) side branch. To calculate $\theta(\epsilon, x)$ we assume Δ is much larger than all the energies integrated in Eq. (4). For the range of the temperature of interest it is good enough to integrate up to $100E_c$. Although this is larger than the actual gap ($\Delta = 32E_c$ using BCS theory), changing Δ in this regime influences the calculation by only a small amount in the region of interest. Figure 7(b) shows the result of the calculation for the total resistance using two different values of Δ . In the regime $\Delta \gg 100E_c$, the curve recovers its normal state value faster at high temperature than the curve obtained from the regime where Δ is close to $100E_c$. At temperatures less than $5E_c$, however, the two regimes do not show a significant difference. Therefore, in our simulations we assume $\Delta \gg 100E_c$.

Regardless of the value of Δ assumed in the calculation, however, it is clear that the proximity effect theory does not describe well the experimental data in the high temperature ($T \leq T_c$) regime, as a comparison with Fig. 2 immediately shows. This is because, near T_c , the contribution from the superconducting transition in the superconducting arm of the loop (which we have ignored so far) must be taken into account. For our control pure Al wire, which has a width of $\sim 0.15 \mu m$, the superconducting transition is fairly sharp, occurring within a range of 5-10 mK. The resistance decrease near T_c seen in Fig. 2, if it is indeed due to the superconducting transition of Al, is much wider. In quasi-one dimensional pure superconducting wires, one mechanism that leads to a finite resistance below the nominal superconducting transition is nucleation of phase-slip centers. The resistance broadening due to these phase-slip centers is given by the Langer-Ambegaokar (LA) form [29]

$$R = \frac{\alpha}{T} \exp \left[-\beta \left(1 - \frac{T}{T_c} \right)^{3/2} / T \right] \quad (6)$$

where α is a parameter associated with the attempt frequency for a phase slip event, and β is a parameter related to the energy barrier for a phase slip event. For pure superconducting wires, β is typically very large ($\sim 10^6$ K) which confines the broadening of the transition to a few millikelvin near T_c [29]. For our N-S structures, since the experimentally measured transition is much broader, β is expected to be much smaller.

Figure 8 shows a comparison between the experimental data (triangles) and the theoretical curve taking into account both the proximity effect and the influence of phase slip centers. The contribution from the proximity effect (dashed line) was obtained as discussed above. The influence of phase slip centers was determined by fitting the difference between the experimental data and the proximity effect contribution to the LA equation (6), using α and β as fitting parameters. The resulting contribution is shown as the dashed line in Fig. 8, with the fitting parameters $\alpha = 0.17 \Omega K$ and $\beta = 9.93$ K. While the contribution due to phase slip centers is significant above 0.6 K, the contribution due to the proximity effect shows a strong temperature dependence only below 0.4 K. The sum of the two contributions is shown as the solid line in the figure, and shows an excellent fit to the experimental data.

We should remark that it is not clear that the theory of phase slip centers should be applicable at all here, although our samples show strong evidence that nonequilibrium phenomena are indeed important near the transition [30]. Nonetheless, our analysis does point to the fact that the value of T_{min} clearly depends on the interplay between the contribution due to the proximity effect in the normal wire and the decrease in resistance of the superconductor near T_c , and consequently, the measured T_{min} will not be simply related to the reentrance effect.

C. Voltage dependence

A similar analysis can be used to calculate the differential resistance $dV/dI = R(V)$ as a function of voltage V . To calculate $R(V)$, one notes the temperature kernel in the integrand of Eq. (2) becomes a step function at $T = 0$ with the discontinuity centered at $\epsilon = eV$, i.e., the contribution to the total current I comes only from $|\epsilon| < eV$ [5]. The conductance dI/dV thus contains a δ -function centered at $|\epsilon| = eV$. This results in a simple formula at $T = 0$ [5]:

$$R(V) = R_N \left(\frac{1}{L} \int_0^L \text{sech}^2 [Im\theta(\epsilon, x)] dx \right)_{\epsilon=eV} \quad (7)$$

This formula is applicable to each branch in Fig. 6(b). In order to calculate the total resistance $R(V)$, however, one must take into account that the voltage V across the entire sample is the sum of the voltages V_1 and V_2 across each individual branch, subject to the condition that the current through both branches is the same. Figure 9 shows the experimental data and the calculated curve based on the procedure outlined above. The agreement between theory and experiment is clearly not satisfactory. The minimum in the experimental resistance occurs at a voltage of $\sim 7.25 \mu V$, while the theoretical curve shows a minimum at $\sim 25 \mu V$. Using the same rationale as for the temperature dependent resistance, we attempt to add the contribution from phase slip centers using the theory of LA [29]. However, with the same parameters obtained in Fig. 8, the curve obtained does not

agree with the experimental data, primarily due to the strong exponential dependence of the theoretical result on the measuring current [29]. There are a number of possible reasons for this disagreement. First, although we think it is essential that nonequilibrium effects need to be taken into account in discussing the voltage dependence, the theory of LA which was developed to discuss phase slip centers in pure superconductors may not adequately describe nonequilibrium phenomena in N-S devices. Second, our calculations assume perfect N and S reservoirs, which are not realized in the experiment. Although this factor might be expected to affect both the temperature and the voltage dependence, indications are that the effect on the voltage dependence might be more significant [31].

D. Magnetoresistance oscillations

The loop in our Andreev interferometers is essential for the observation of magnetoresistance oscillations, and hence cannot be ignored in any calculation of the magnetoresistance. This complicates the calculation tremendously. Consequently, we have not attempted to numerically solve the quasiclassical Green's function equations in the presence of a magnetic field. However, the qualitative behavior can be understood by drawing on our experience with other quantum interference phenomena in doubly-connected geometries. For the case of weak localization in single normal metal rings, for example, the magnetoresistance oscillates as a function of magnetic field with fundamental period $h/2e$ [32]. The oscillations are suppressed exponentially with the phase coherence length L_φ , $\exp(-L/L_\varphi)$, where L is the perimeter of the loop. In our Andreev interferometers, quantum coherence is maintained in the superconducting arms of the loop. In the normal arm, the oscillation amplitude is determined by the phase coherence length ξ_N . Since the normal arm is connected to the superconductor on both sides, the suppression of the oscillation amplitude might be expected to go as $\sim \exp[-L/(2\xi_N)]$, where L is now the length of the normal arm. This exponential dependence is what we indeed observe in sample A, and also in sample B at higher temperatures. The reentrance effect we see in the amplitude of the magnetoresistance oscillations

in sample B is an indication that these oscillations are dependent on the enhancement of the diffusion coefficient in the normal arm of the loop.

V. CONCLUSION

In conclusion, we have investigated the reentrance effect in two mesoscopic N-S hybrid loops with different interface transparencies. The low transmittance sample showed no reentrant behavior, consistent with the fact that the relevant energy and temperature scales were shifted to values below our measurement range. The high transmittance sample, on the other hand, showed reentrant behavior in $R(T)$, $dV/dI(V)$, and amplitude of magnetoresistance oscillations, due to the long range coherence of the electron-hole pairs induced by Andreev reflection at the N-S interfaces. A quantitative understanding of the experimental results cannot be obtained from the quasiclassical Green's function theory of reentrance alone. For a more complete quantitative understanding of the properties of such N-S devices, we believe it is essential to understand the effect of nonequilibrium phenomena on the transport properties, particularly at high bias voltages or near the transition temperature of the superconductor.

ACKNOWLEDGMENTS

We acknowledge useful discussions with Sungkit Yip and John Ketterson, and thank Michael Black for a critical reading of the manuscript. Work at Northwestern was supported by the NSF under DMR-9357506, and by the David and Lucile Packard Foundation.

REFERENCES

- [1] See, for instance, G. Deutscher and P. G. De Gennes, in *Superconductivity* edited by R. D Parks (Marcel Dekker, New York, 1969).
- [2] A. F. Andreev, Sov. Phys. JETP **19**, 1228 (1964).
- [3] S. N. Artemenko, A. F. Volkov, and A. V. Zaitsev, Solid State Comm. **30**, 771 (1979).
- [4] Y. V. Nazarov, Phys. Rev. Lett. **73**, 1420 (1994).
- [5] S. Yip, Phys. Rev. **B52**, 15504 (1995).
- [6] Y. V. Nazarov and T. H. Stoof, Phys. Rev. Lett. **76**, 823 (1996).
- [7] A. F. Volkov, N. Allsopp, C. J. Lambert, J. Phys.:Cond. Matt. **8**, L45 (1996).
- [8] A. A. Golubov, F. K. Wilhelm, and A. D. Zaikin, Phys. Rev. **B55**, 1123 (1997).
- [9] A. F. Volkov, A. V. Zaitsev and T. M. Klapwijk, Physica C **210**, 21 (1993) ; A. F. Volkov, Physica B **203**, 267 (1994) and references therein.
- [10] H. Courtois, Ph. Gandit, D. Mailly and B. Pannetier, Phys. Rev. Lett. **76**, 130 (1996).
- [11] P. Charlat, H. Courtois, Ph. Gandit, D. Mailly, A. F. Volkov, and B. Pannetier, Phys. Rev. Lett. **77**, 4950 (1996); Czech J. Physics, V **46**, 3107 (1996).
- [12] V. T. Petrashov, R. Sh. Shaikhaidarov and I. A. Sosnin, JETP Lett. **64**, 840 (1996).
- [13] S. G. Den Hartog, C. M. A Kapteyn, B. J. Van Wees, T. M. Klapwijk and G. Borghs, Phys. Rev. Lett. **77**, 4954 (1996).
- [14] S. G. den Hartog, B. J. Van Wees, Y. V. Nazarov, T. M. Klapwijk, and G. Borghs, preprint (1997).
- [15] E. Toyoda and H. Takayanagi, The 12th International Conference on the Electronic Properties of Two-Dimensional Systems, EP2DS-12 (Tokyo September 1997).

- [16] V. N. Antonov, A. F. Volkov and Hideaki Takayanagi, Europhys. Lett., **38(6)**, 453 (1997).
- [17] V. N. Antonov, A. F. Volkov and Hideaki Takayanagi, Phys. Rev. **B55**, 3836 (1997).
- [18] A. F. Volkov and A. V. Zaitsev, Phys. Rev. **B53**, 9267 (1996).
- [19] L_φ is estimated from weak localization measurements on co-evaporated normal metal control wires. We believe L_φ for the Ag wire is very short due to the bake required for the second layer of the lithography.
- [20] P. G. N. De Vegvar, T. A. Fulton, W. H. Mallison, and R. E. Miller, Phys. Rev. Lett. **73**, 1416 (1994).
- [21] H. Pothier, S. Gueron, D. Esteve, and M. H. Devoret, Phys. Rev. Lett. **73**, 2488 (1994).
- [22] A. Dimoulas, J. P. Heida, B. J. v. Wees, T. M. Klapwijk, W. v. d. Graaf, and G. Borghs, Phys. Rev. Lett. **74**, 602 (1995).
- [23] V. T. Petrashov, V. N. Antonov, P. Delsing, and T. Claeson, Phys. Rev. Lett. **74**, 5268 (1995).
- [24] S. G. den Hartog, C. M. A. Kapteyn, B. J. v. Wees, T. M. Klapwijk, W. v. d. Graaf, and G. Borghs, Phys. Rev. Lett. **76**, 4592 (1996).
- [25] A. Kastalsky, A. W. Kleinsasser, L. H. Greene, R. Bhat, F. P. Milliken and J. P. Harbison, Phys. Rev. Lett. **67**, 3026 (1991).
- [26] B. J. van Wees, P. de Vries, P. Magnee and T. M. Klapwijk, Phys. Rev. Lett. **69**, 510 (1992).
- [27] K. D. Usadel, Phys. Rev. Lett. **25**, 507 (1970).
- [28] T. H. Stoof and Yu. V. Nazarov, Phys. Rev. **B53**, 14496 (1996).
- [29] See, for example, M. Tinkham, *Introduction to Superconductivity*, 2nd edition.

(McGraw-Hill, New York, 1996). The correction introduced by McCumber and Halperin is not important for our discussion.

[30] C.J. Chien and V. Chandrasekhar, unpublished.

[31] H. Courtois, private communication.

[32] See, for example, S. Washburn and R.A. Webb, *Adv. Phys.* **35**, 375 (1986).

FIGURES

FIG. 1. (a) Scanning electron micrograph of sample A. The additional gate electrode was kept grounded and not used in these measurements. (b) Sample schematics for the two samples. The dimensions are indicated in μm . The leads used to applied ac currents and measure the voltages are also shown in the schematics. For the dV/dI measurements, an additional dc current is applied through I+/-.

FIG. 2. The normalized resistance R/R_N for samples A and B as a function of temperature T . $R_N=67.5\ \Omega$ and $10.3\ \Omega$ for samples A and B respectively.

FIG. 3. (a), (b) are the magnetoresistance curves $R(H)$ for sample A and B respectively. The small offset of H in (a) is due to the residual flux trapped in the superconducting magnet. In (a) the curves for $T=101\ \text{mK}$, $203\ \text{mK}$, $400\ \text{mK}$ and $1.07\ \text{K}$ are shifted up by $4\ \Omega$, $8\ \Omega$, $12\ \Omega$, and $16\ \Omega$ respectively. In (b) the curves for $T = 97\ \text{mK}$, $199\ \text{mK}$, $491\ \text{mK}$ and $600\ \text{mK}$ are shifted up by $0.2\ \Omega$, $0.4\ \Omega$, $0.7\ \Omega$ and $0.8\ \Omega$ respectively. (c) Normalized amplitude of the Fourier transform of (a) and (b) as a function of temperature. The field range is $\pm 25\ \text{mT}$ and $\pm 20\ \text{mT}$ and the normalization constant is $0.982\ \Omega$ and $0.019\ \Omega$ for samples A and B respectively. The solid lines represent fits to the form $a \exp(-bT^{1/2})$ at higher temperatures, with $a = 3.1, 2.7$ and $b = 3.4, 2.2$ for samples A and B respectively. For comparison, we also show a best fit to a power law of the form a/T as used by Courtois *et al.* [10], with the values $a=0.128, 0.238$ for samples A and B respectively.

FIG. 4. Normalized dV/dI as a function of dc voltage V at $T=30\ \text{mK}$ for sample A (solid curve) and B (dotted curve). The voltage is obtained by integrating dV/dI vs. I_{dc} . ac and dc currents are applied through I+/- shown in Fig. 1(b). $(dV/dI)_N$ is $67.5\ \Omega$ and $10.3\ \Omega$ for samples A and B respectively. The dashed curve shows dV/dI for sample A at a magnetic field of $225\ \text{gauss}$.

FIG. 5. $R(T)$ measured for (a) sample A, and (b) sample B at various values of integral and half-integral flux quanta $h/2e$ through the loop. Closed symbols, integral flux quanta, open symbols, half-integral flux quanta. The temperature dependent curves were obtained from data similar to that of Fig. 3.

FIG. 6. Schematic of the simulated model. (a) Actual sample. (b) Geometry used in the calculation.

FIG. 7. Simulation of the resistance as a function of temperature based on the model in Fig. 6. (a) Resistance as a function of temperature for R_1 , R_2 and $R = R_1 + R_2$, assuming $\Delta \gg E_c$. (b) Total resistance R as a function of T for different Δ 's. $\Delta = 200E_c$, 10^4E_c for the solid curve and dashed curve respectively.

FIG. 8. Theoretical fit to $R(T)$ combining the predictions of the quasiclassical Green's function theory with the phase slip model of Langer and Ambegaokar [29], as discussed in the text. The parameters used in the fit (referring to Eq. (6)) are $\alpha = 0.17 \text{ } \Omega\text{K}$, and $\beta = 9.93 \text{ K}$, $T_c = 1.2 \text{ K}$. The dotted curve which represents the prediction of the quasiclassical Green's function theory, is shifted down by $0.04 \text{ } \Omega$ and the dashed curve, which represents the predictions of the phase slip model of LA is shifted up by $0.45 \text{ } \Omega$ for clarity.

FIG. 9. Comparison of the theoretical calculation (solid curve) based on the theory of quasiclassical Green's functions with the measured $dV/dI(V)$ (triangles). The dashed curve shows the effect of adding the predictions of the LA theory using the same parameters as in Fig. 8.

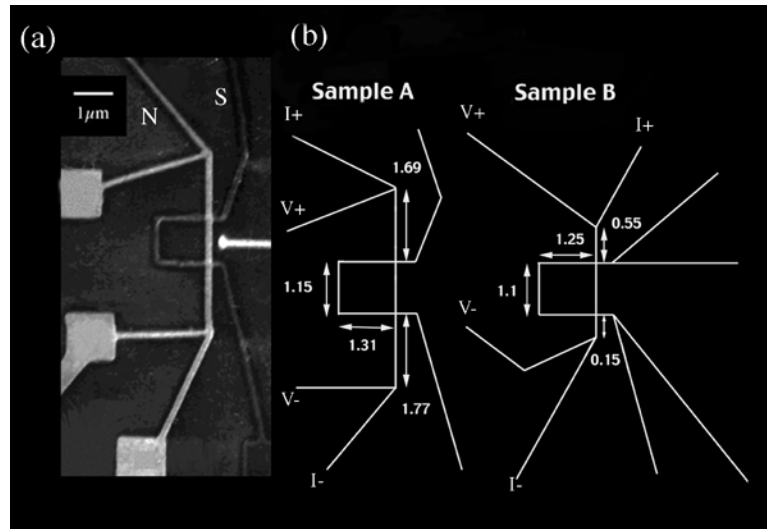


Fig. 1
Chien et al

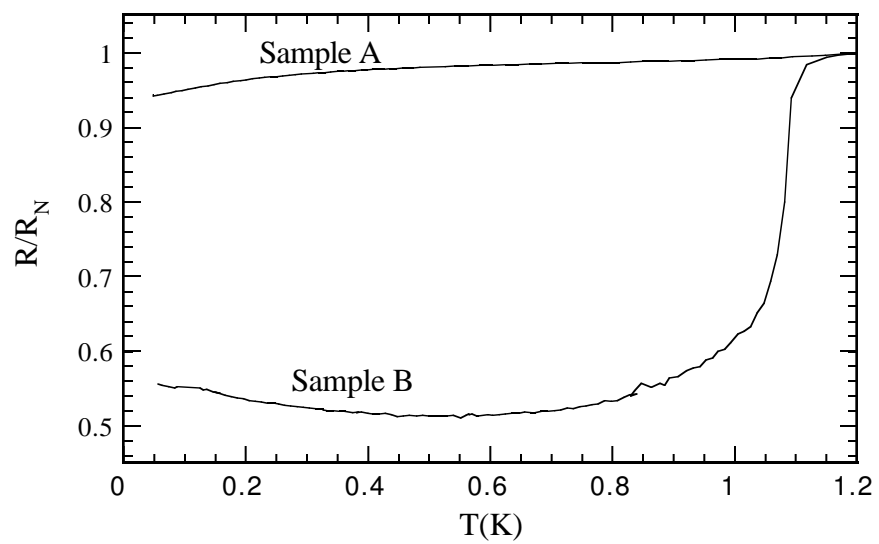
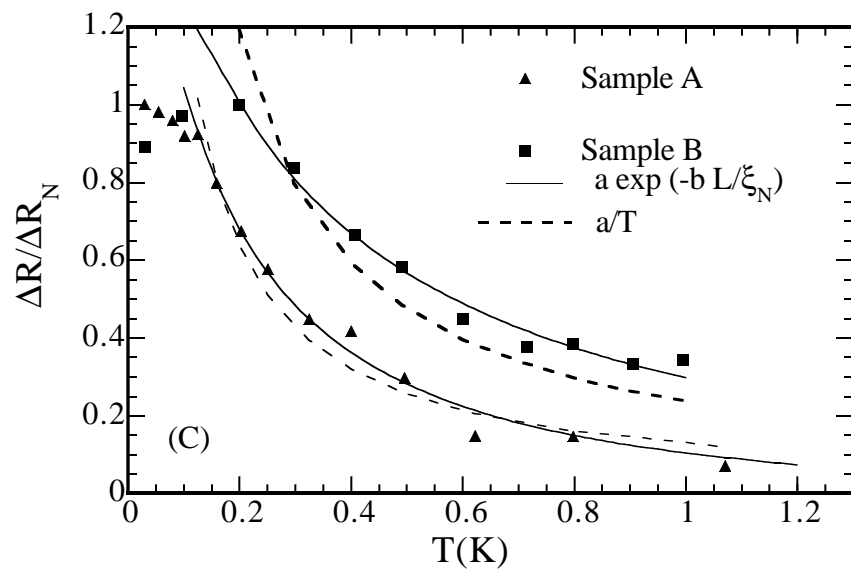
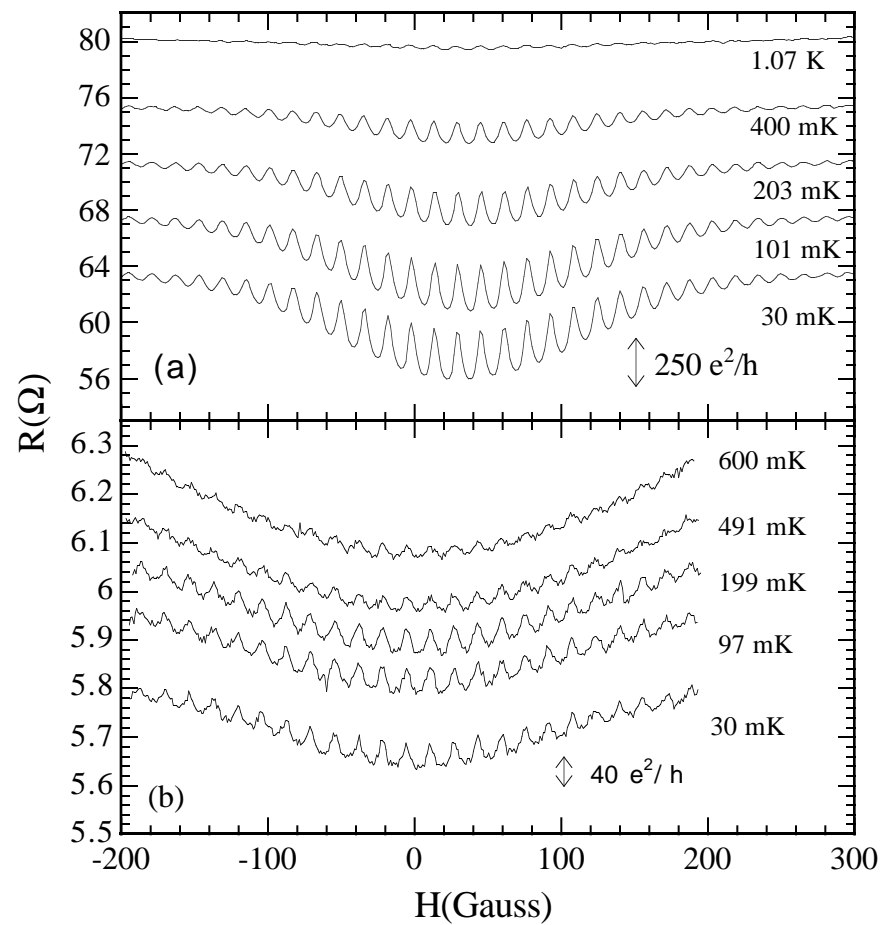


Fig 2
Chien et al



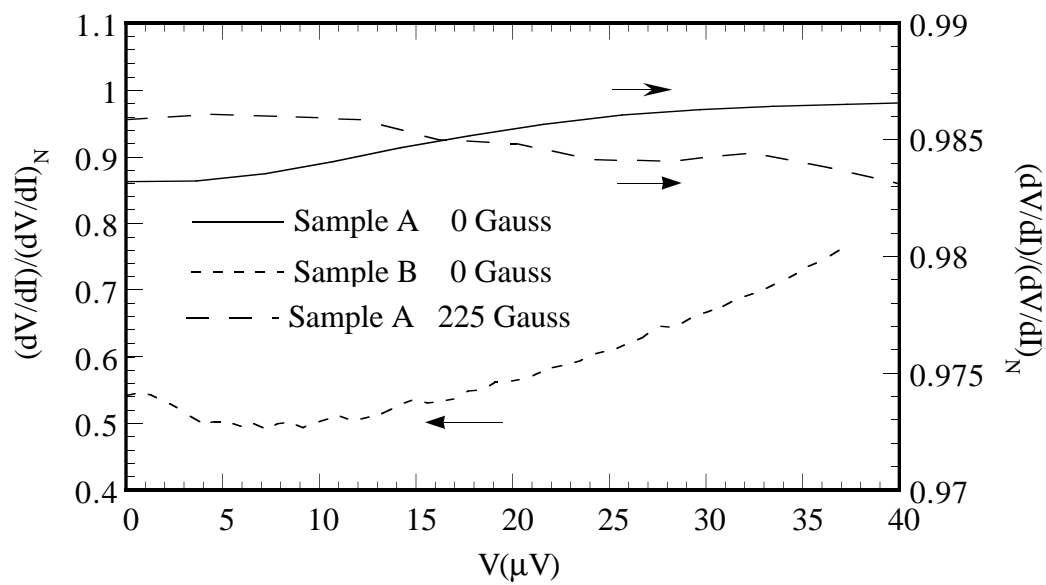


Fig. 4
Chien et al

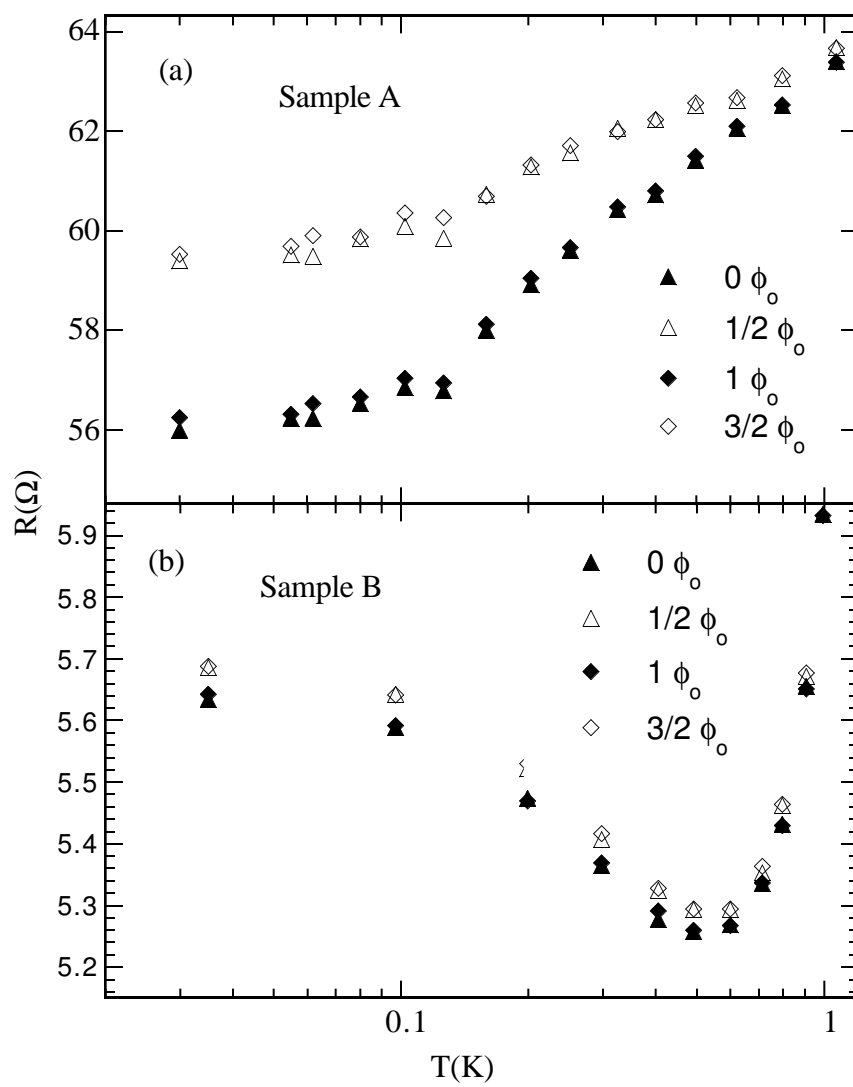


Fig. 5
Chien et al

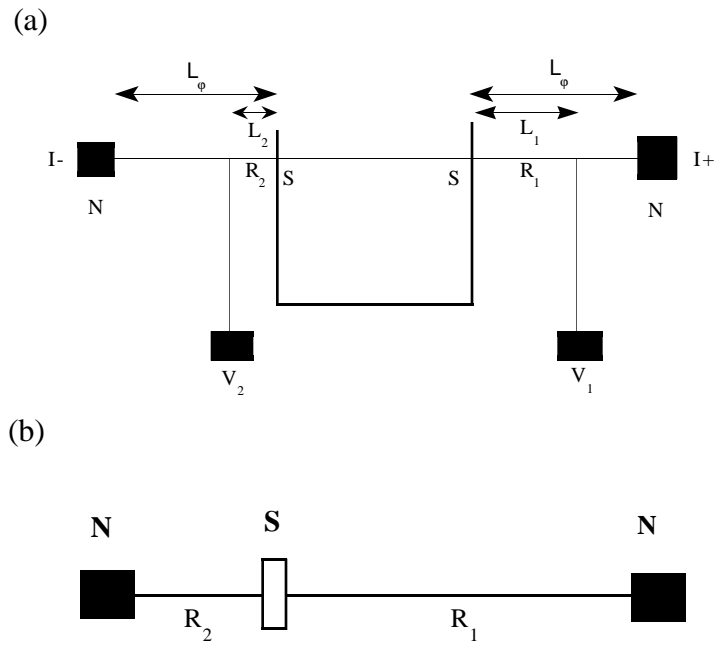


Fig. 6 Chien et al

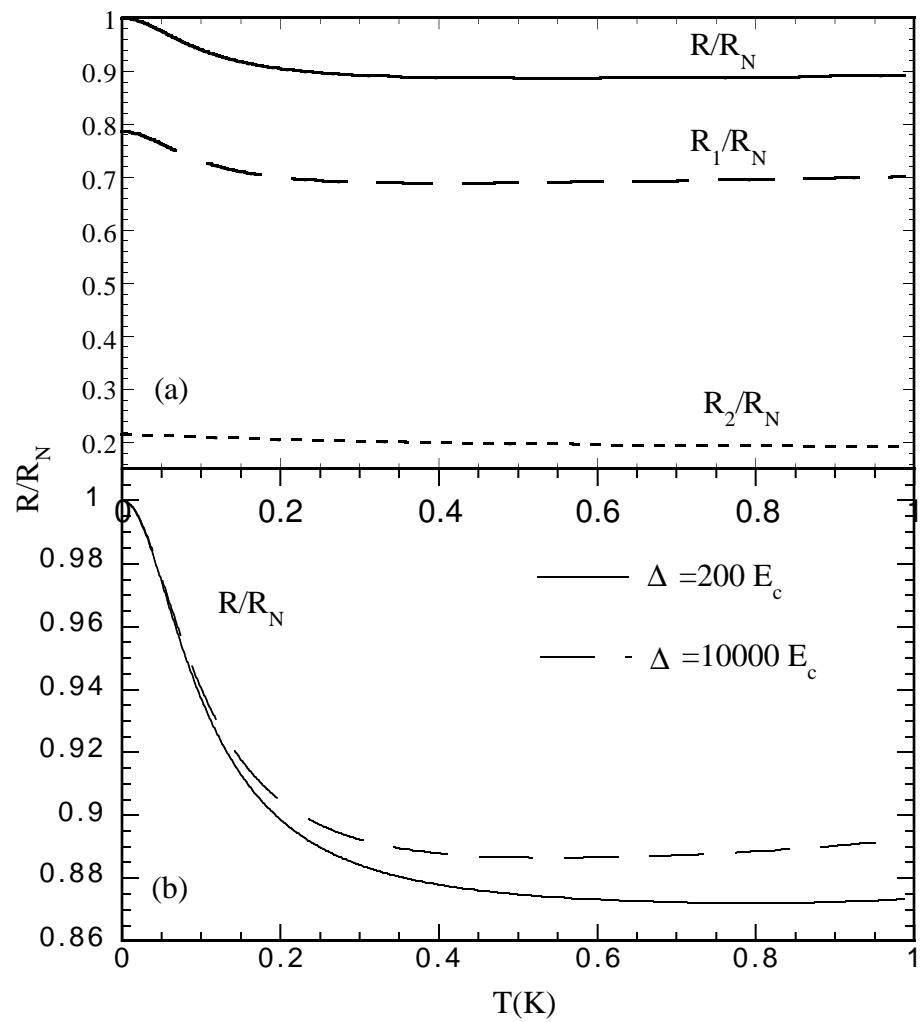


Fig. 7
Chien et al

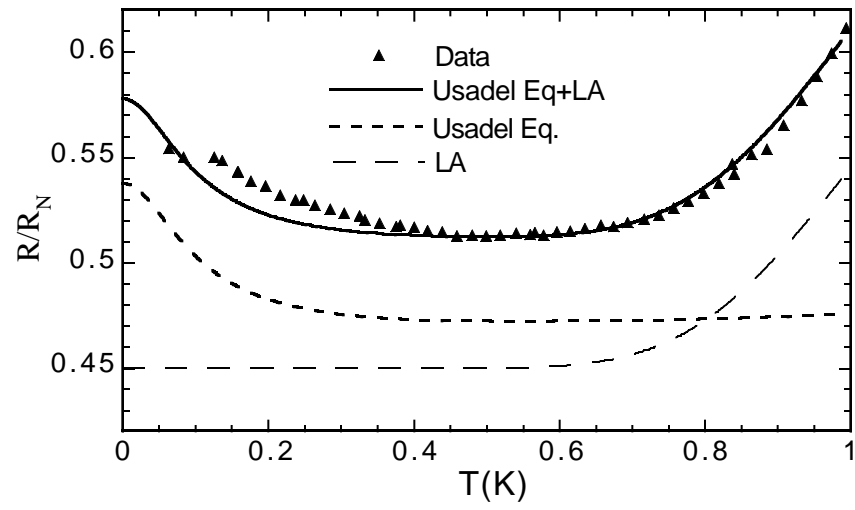


Fig. 8
Chien et al

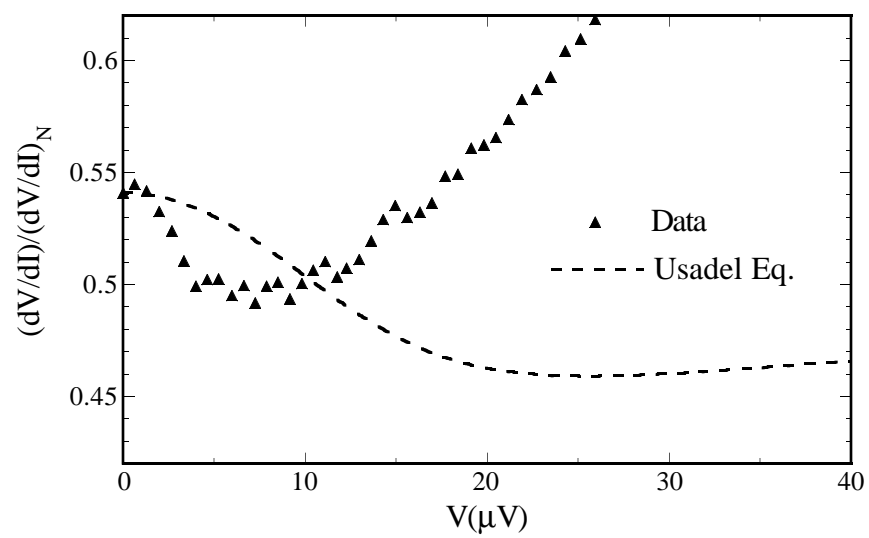


Fig. 9
Chien et al